Geothermics 112 (2023) 102730

Contents lists available at ScienceDirect

Geothermics

journal homepage: www.elsevier.com/locate/geothermics

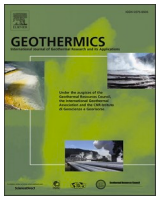

Friction and stability of granite faults in the Gonghe geothermal reservoir and implications for injection-induced seismicity

Fengshou Zhang [a,b], Shutian Cao [a,b], Mengke An [a,b,*], Chongyuan Zhang [c], Derek Elsworth [d,e]

[a] Department of Geotechnical Engineering, College of Civil Engineering, Tongji University, Shanghai 200092, China
[b] Key Laboratory of Geotechnical & Underground Engineering of Ministry of Education, Tongji University, Shanghai 200092, China
[c] Key Laboratory of Neotectonic Movement and Geohazard, Institute of Geomechanics, Chinese Academy of Geological Sciences, Beijing 100081, China
[d] Department of Energy and Mineral Engineering, EMS Energy Institute and G3 Center, The Pennsylvania State University, University Park, PA 16802, USA.
[e] Department of Geosciences, The Pennsylvania State University, University Park, PA 16802, USA.

ARTICLE INFO

Keywords:
Enhanced geothermal system
Granite faults
Frictional stability
Hydrothermal conditions
Hydraulic fracturing
Induced seismicity

ABSTRACT

The Gonghe Basin in northwest China has significant potential for the recovery of deep geothermal fluids. However, a large number of earthquakes were observed during stimulation by hydraulic fracturing with the maximum magnitude reaching ~ M_L 2. To understand the mechanisms of deep fault stability and the clusters of earthquakes, we recovered seven granite cores from the Gonghe geothermal reservoir and powdered them to simulate fault gouges. XRD results show that the granites are dominated by quartz and feldspar and show a high chlorite content. Triaxial shear experiments were conducted on the seven gouges to explore the frictional and stability properties at conditions typifying the depths of 2450–3600 m in the Gonghe geothermal site. Results show that the friction coefficients of the tested gouges are high and close to 0.70. At hydrothermal conditions, all gouges show slight velocity-weakening to velocity-neutral behavior, which is indicative of potentially unstable fault slip. Our results have important implications for understanding the fault stability behavior and induced seismicity during hydraulic fracturing in granite geothermal reservoirs.

1. Introduction

The Gonghe Basin, located in the transition zone between the Qilian and Kunlun Mountains of northwest China (Fig. 1), is host to a pilot study for hot dry rock geothermal energy development (Liu et al., 2020). This area has a high geothermal gradient (~64 °C/km) due to magmatic activity, especially in the northeastern part of the Qabaq region. One well (GR1) has a bottom hole temperature of 236 °C at a depth of 3705 m. Moreover, the recoverable resource from hot dry rock in the Qabaq region is estimated to be >30 EJ - equivalent to >1 billion tons of coal (Zhang et al., 2018). These characteristics make the Gonghe Basin one of the most promising geothermal development sites in China (Zhu et al., 2015).

Hydraulic fracturing or hydraulic shearing of pre-existing fractures is typically applied to the recovery of deep geothermal resources. Hydraulic fracturing, which involves a massive fluid injection of high-pressure fluids into the subsurface can greatly enhance reservoir permeability and improve heat exchange efficiency. However, the fluid injection necessarily increases pore fluid pressures and may result in the unplanned reactivation of pre-existing faults/fractures and induce earthquakes (Pearson, 1981; Zoback and Harjes, 1997; Majer et al., 2007; Passelègue et al., 2018; Ye and Ghassemi, 2018; Ji et al., 2022; Scuderi et al., 2017; Zhang et al., 2022).

The exploitation of geothermal reservoirs worldwide is always accompanied by induced seismic hazards that threaten the public acceptance of EGS (Enhanced Geothermal System). The power generation capacity of the EGS project in Soultz (France) has reached the megawatt level, regarded as the most successful geothermal reservoir (Breede et al., 2013). Nevertheless, more than 400 microearthquakes with a maximum magnitude of M_w 2.9 have occurred in the geothermal reservoir of Soultz (Majer et al., 2007). The 'Basel' project (Switzerland) was suspended owing to observed induced seismic events among which some exceeded M_w 3.0 (Ladner and Häring, 2009). Pohang EGS site (South Korea) is known for the largest induced earthquake of M_w 5.5 in November 2017 during hydraulic stimulation, leading to significant damage and public attention (Kim et al., 2018). Similarly, during the stimulation of well GR1, the maximum moment magnitude of near-field earthquakes reached ~ M_w 3 (Chen et al., 2021). Considering the

* Corresponding author.
E-mail address: 2015mengkean@tongji.edu.cn (M. An).

https://doi.org/10.1016/j.geothermics.2023.102730
Received 20 September 2022; Received in revised form 5 April 2023; Accepted 23 April 2023

promising development potential of the Gonghe Basin, it is of great importance to understand the underlying mechanisms of induced earthquakes during geothermal exploitation – to promote the control and mitigation of seismic hazards.

Granite is a common basement host for many geothermal reservoirs, worldwide, including those at Soultz (France), Pohang (South Korea), Coso (USA) and in the Gonghe Basin (China) (Majer et al., 2007; Vidal and Genter, 2018; Kovac et al., 2005; Kim et al., 2018; Grigoli et al., 2018), and granite faults are reported to be velocity-weakening at hydrothermal conditions, contributing to unstable slip and induced seismicity (e.g., Stesky, 1978; Lockner et al., 1986; Blanpied et al., 1991, 1995; Mitchel et al., 2016; Kolawle et al., 2019; Kang et al., 2021; An et al., 2022). Thus, systematically characterizing the frictional properties of granite faults at hydrothermal conditions typifying a geothermal reservoir is needed to better understand the seismic behavior in reservoir granite faults.

In this work, we first analyze the main components of granites recovered from well GR1 of the Gonghe Basin, then conduct laboratory shear experiments on the granite gouges to characterize the frictional and stability properties at *in-situ* hydrothermal conditions of the Gonghe geothermal reservoir, in order to obtain a better understanding of the seismic possibility and nucleation mechanism in granite faults within the Gonghe Basin

2. Experimental methods

2.1. Sample preparation

We collected seven granitic cores (numbers: 245#, 255#, 290#, 325#, 340#, 350# and 360#) from well GR1 at depths between 2450 and 3600 m (Fig. 2). After removing drilling-debris, all granites were powdered and then sieved to particle sizes <75 μm to simulate the fault gouges. The mineral compositions of the granites were analyzed by X-ray diffraction (XRD) with the results reported in Table 1. Primary components are quartz, albite, microcline, chlorite and biotite, with traces of amphibole and calcite. The quartz content first increases then decreases with increasing depth while albite shows the opposite trend. The chlorite content generally increases with depth (except for sample 360#) but biotite content decreases.

Bare or carved fractures and simulated gouges are both capable of demonstrating the frictional properties of faults/fractures at different failure stages (Moore et al., 1994; Morrow et al., 2001). Fault gouges, resulting from brittle fragmentation and wear, are typically observed within large tectonic faults at seismic cycles (Scholz, 1990; Carpenter et al., 2016). Generally, fault gouge is a common product of nearly all near-surface faulting regardless of the size and location (Vrolijk and van der Pluijm, 1999), and is reported to show a vital control on fault stability and earthquake nucleation (Brace and Byerlee, 1966; Johnson et al., 1973; Marone et al., 1990). In addition, shear within gouge-filled faults exhibits lower rupture velocities, more precursory slip before

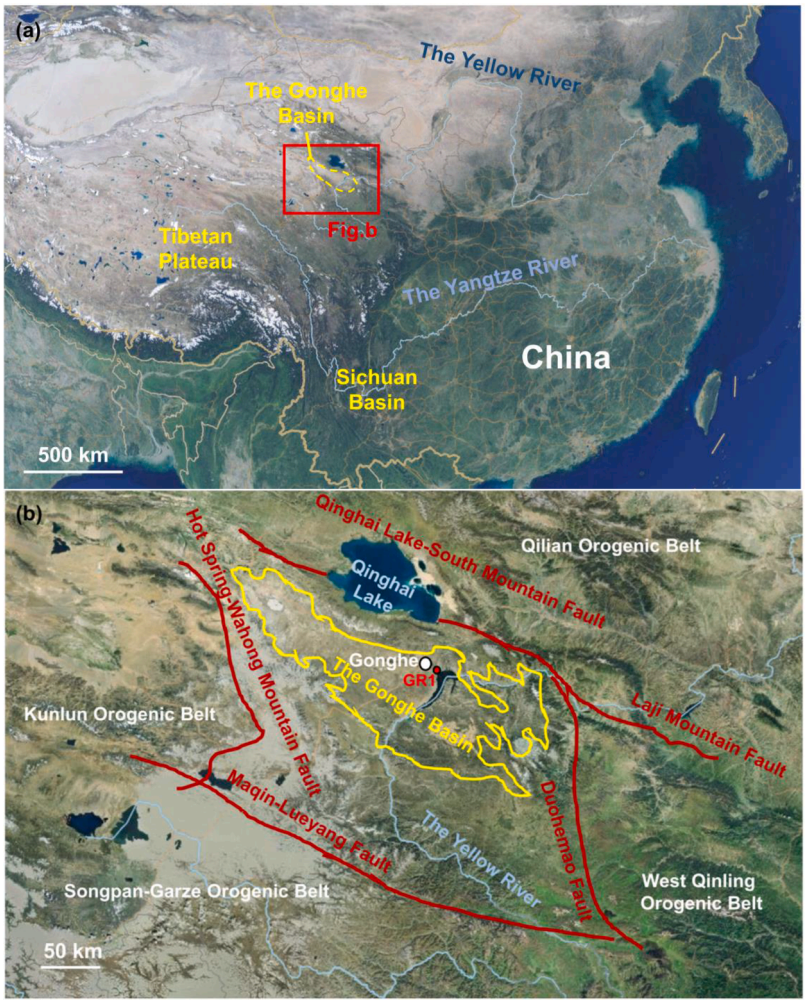

Fig. 1. (a) Location of the Gonghe Basin (yellow dashed line, coordinates: 98.46–101.22°E, 35.27–36.56°N). Red rectangle in (a) indicates the area of panel (b). (b) Surrounding orogenic belts and faults of the Gonghe Basin. Both figures are derived from Baidu Maps.

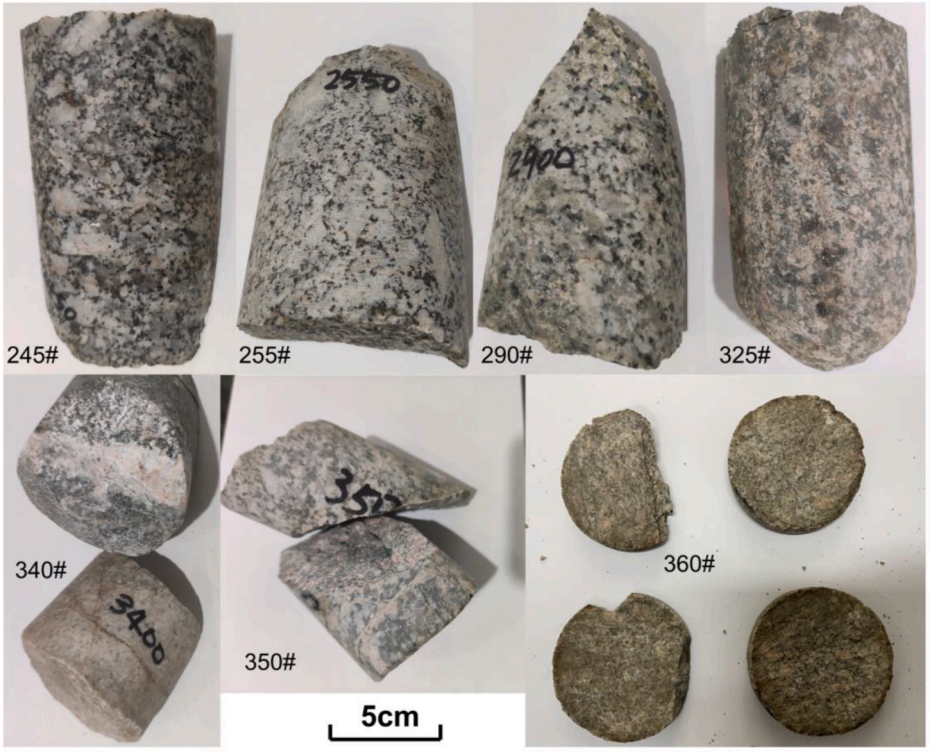

Fig. 2. Granite core fragments recovered from well GR1.

Table 1
Mineral compositions (wt.%) of the collected granites. Sample numbers refer to sample depths in the range 2450–3600 m in well GR1.

Granite numbers	245#	255#	290#	325#	340#	350#	360#
Quartz	32	34	39	44	39	29	32
Albite	43	26	21	12	24	20	31
Microcline	8	13	12	1	5	9	21
Chlorite	3	2	25	23	29	39	11
Biotite	9	18	3	9	3	3	3
Amphibole	5	7	–	–	–	–	–
Calcite	–	–	–	11	–	–	2

rupture nucleation and larger nucleation zones compared to that of bare fractures/faults (Marone and Kilgore, 1993; Buijze et al., 2020; Beeler et al., 2022; Giacomel et al., 2021). Thus, we chose simulated fault gouge mainly to match the apparatus (He et al., 2006), the fault gouge can also characterize the fault frictional properties to a certain extent and lead to more stable curves.

The particle-size distribution can also determine the gouge strength to some content – particle comminution is driven by relative movement among particles and controlled by neighbor particle size, and smaller particles dominate gouge weakening within shear localizations (Marone and Scholz, 1989). The reduction of d_c values is also caused by particle size decrease through comminution (Marone and Kilgore, 1993). To acquire more accurate results, we chose proper particle sizes typifying common natural gouges with small-scale fractures to simulate shearing gouges (i.e., <75 μm) (Roux et al., 1993), which simultaneously accommodates to the triaxial apparatus conditions (He et al., 2006).

It is worth noting that the granites from well GR1 are generally rich in chlorite. The granites at depths of 2900–3500 m have chlorite contents >20 wt.%. Chlorite is a common low-grade metamorphic mineral in shallow geothermal reservoirs (Kwon et al., 2019; Bird and Spieler, 2004). The abundance of chlorite in the Gonghe Basin is likely a result of magmatic activity or from the metamorphism of amphibole or biotite (Talarico and Kleinschmidt, 2003; Sun and Colin, 2014; Wehrens et al., 2016)

2.2. Testing procedure

Shear experiments were conducted using an argon-gas confined triaxial shear apparatus (Fig. 3) at the Institute of Geology, China Earthquake Administration, Beijing, China. This apparatus can apply a maximum temperature of 600 °C, a maximum confining pressure of 420 MPa and a maximum pore fluid pressure of 200 MPa. A 1-mm thick layer of gouge was sandwiched between two gabbro driving blocks (20-mm diameter and 40-mm height) with a saw cut inclined at 35° to the loading axis. An injection hole was drilled through the upper gabbro block for pore fluid entry, and a brass filter was placed within the hole to prevent gouge extrusion. The sawcut surfaces of the two blocks avoid boundary slippage and were both polished by 200-mesh silicon carbide. The cylindrical gabbro block assembly with the intervening gouge was inserted into a 0.35-mm thick annealed copper jacket, with tungsten carbide then high-hardness corundum forcing blocks placed top and bottom. Two O-rings top and bottom of the assembly seal the copper jacket and prevent the gas leakage during the experiment. The sample assembly within the copper jacket is ringed by a furnace and placed in a confining vessel with the space between the furnace and jacket filled with boron nitride to avoid gas convection. A thermocouple was inserted into the pore fluid entry port to monitor the gouge temperature at midpoint (Fig. 3).

The confining pressure was applied by argon gas with the pressurized pore fluid comprising deionized water, similar to typical triaxial shear-flow tests (Jiang et al., 2022). At the beginning of each test, both the confining and pore fluid pressures were applied to about two thirds of the target values to allow heating at a rate of 5 °C/min to the desired temperature. Finally, the confining and pore fluid pressures were adjusted to the target values and kept constant within ±0.5 MPa and ±0.3 MPa, respectively. Axial deformation was applied with an electrohydraulic servo-controlled system and the axial displacement was recorded by an independent displacement sensor.

Seven shear experiments (Test ID: G245, G255, G290, G325, G340,

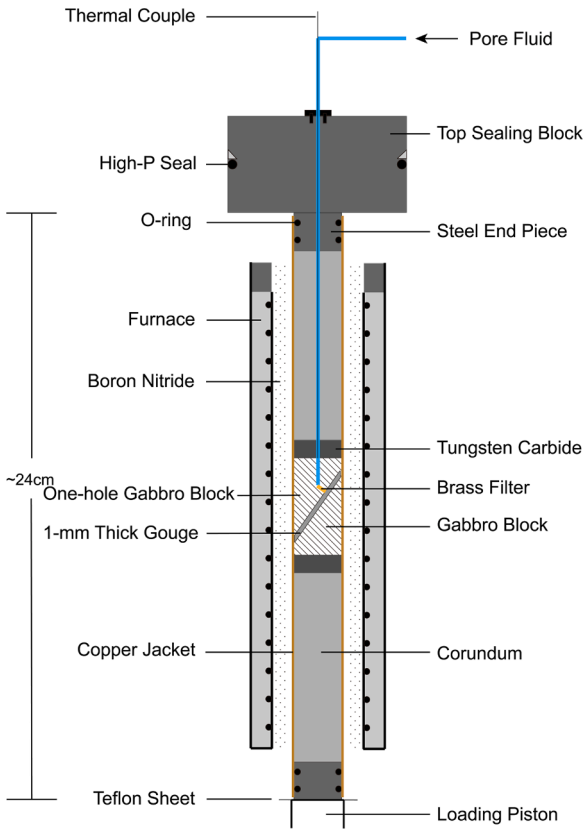

Fig. 3. Schematic of the triaxial shear apparatus.

G350 and G360 corresponding to depths 2450–3600 m in well GR1) were conducted on the powdered gouges from seven depth intervals to characterize the frictional strength and stability under hydrothermal conditions - with experiment details noted in Table 2. Confining and pore fluid pressures approximate the lithostatic (rock density of ~2500 kg/m^3) and hydrostatic (water density of ~1000 kg/m^3) pressures between 2.45–3.6 km, respectively. Experimental temperatures were determined from well GR1 temperature data reported by Zhang et al. (2018). Considering the uneven temperature distribution even on the same horizontal level, two additional tests (Test IDs: G245t and G340t) were completed on samples G245 and G340 at elevated temperatures to ensure integrated results and evaluate temperature dependence. All gouges were sheared at an initial axial displacement rate of 1 μm/s until reaching steady state friction. Then the axial loading rate was stepped in the schedule 1–0.2–0.04–0.2–1–0.2–0.04 μm/s equivalent to shear velocities of 1.22–0.244–0.0488–0.244–1.22–0.244–0.0488 μm/s within the gouge, we conducted such velocity-stepping experiments to determine the rate dependence and finally frictional stability of granite fault gouges

Table 2
Matrix of experimental conditions. σ_c = confining pressure, P_f = pore fluid pressure, T = temperature, and designation of l_{final} = final shear displacement and response as either vs = velocity-strengthening or vw = velocity-weakening.

Testing ID	Granite gouges	σ_c (MPa)	P_f (MPa)	T (°C)	l_{final} (mm)	Fault response
G245	245#	60	25	150	2.99	vs, vw
G255	255#	65	25	150	3.26	vw
G290	290#	70	30	175	3.40	vw
G325	325#	80	30	200	3.22	vs
G340	340#	85	35	215	3.42	vs
G350	350#	85	35	220	3.27	vs, vw
G360	360#	90	35	230	3.65	vs, vw
G245t	245#	60	25	185	2.77	vw
G340t	340#	85	35	250	3.54	vs

2.3. Data analysis

The experimental data, including the confining pressure, pore fluid pressure, axial displacement, piston load and temperature were recorded at a sampling frequency of 1-Hz. Then the raw experimental data were corrected to eliminate the effect of the reduced contact area with increasing shear offset together with the shear resistance of the copper jacket using the method described in He et al. (2006). The coefficient of friction μ was calculated as

$$\mu = \frac{\tau}{\sigma_{neff}} = \frac{\tau}{(\sigma_n - P_f)} \tag{1}$$

where τ and σ_n represent the corrected shear and normal stresses, respectively, σ_{neff} denotes the effective normal stress. The velocity dependence parameter (a - b) was obtained from rate and state friction (RSF) theory (Dieterich, 1979; Rice, 1983; Ruina, 1983). In the framework of RSF theory, the coefficient of friction μ is expressed as,

$$\mu = \mu_0 + aln\left(\frac{V}{V_0}\right) + bln\left(\frac{V_0\theta}{d_c}\right) \tag{2}$$

$$\frac{d\theta}{dt} = 1 - \frac{V\theta}{d_c} \tag{3}$$

where μ_0 is the coefficient of friction at the reference shear velocity V_0, V is the instantaneous shear velocity of the up/down-step, a and b are dimensionless constants that denote the direct and evolutional effects in a velocity step, respectively, d_c is the critical slip distance required to reach a new steady state, and the state variable θ indicates the contact age. At steady state, Eq.(3) reduces to $V\theta = d_c$. Thus, the velocity dependence parameter (a - b) can be calculated from,

$$a - b = \frac{\mu - \mu_0}{ln(V/V_0)} = \frac{\Delta\mu_{ss}}{\Delta lnV} \tag{4}$$

where μ_{ss} represents the difference of the coefficient of friction between two successive steady states. A positive (a - b) denotes stable sliding and velocity-strengthening behavior - conversely a negative (a - b) indicates velocity-weakening behavior and the potential for unstable sliding whenever the critical stiffness criterion is also met.

3. Results & discussion

3.1. Frictional strength and stability

The friction-displacement curves for the seven experiments (Testing ID: G245, G255, G290, G325, G340, G350 and G360) under hydrothermal conditions are presented in Fig. 4. At shear displacements of 1.0–1.5 mm, all gouges are approaching their steady state and then show a slight strain-hardening trend, revealing sustained grain crushing and gouge evolution (Tembe et al., 2010). All curves have been detrended before estimating values of (a - b) to eliminate the effect of strain-hardening. Tests G245 and G255 show apparent stick-slip at the lowest shear velocity of 0.0488 μm/s, indicating a potential seismic response (Brace and Byerlee, 1966).

Results for the coefficient of friction (μ) and the frictional stability (a - b) for the seven gouges are presented in Figure 5. The coefficient of friction of the seven gouges (except for G325) all approach 0.70, similar to other granite gouges reported by An et al. (2021) and Blanpied et al. (1995). The lower frictional strength (~0.61) in G325 possibly results from the lowest tectosilicate content (~57 *wt.*% quartz + albite + microcline) (Ikari et al., 2009). Frictional stability (a - b) was calculated following the methods described in Section 2.3 with the results shown in Fig. 5b. Values of (a - b) for the seven gouges are within −0.0100 to 0.0050, indicating velocity-neutral to slight velocity-weakening

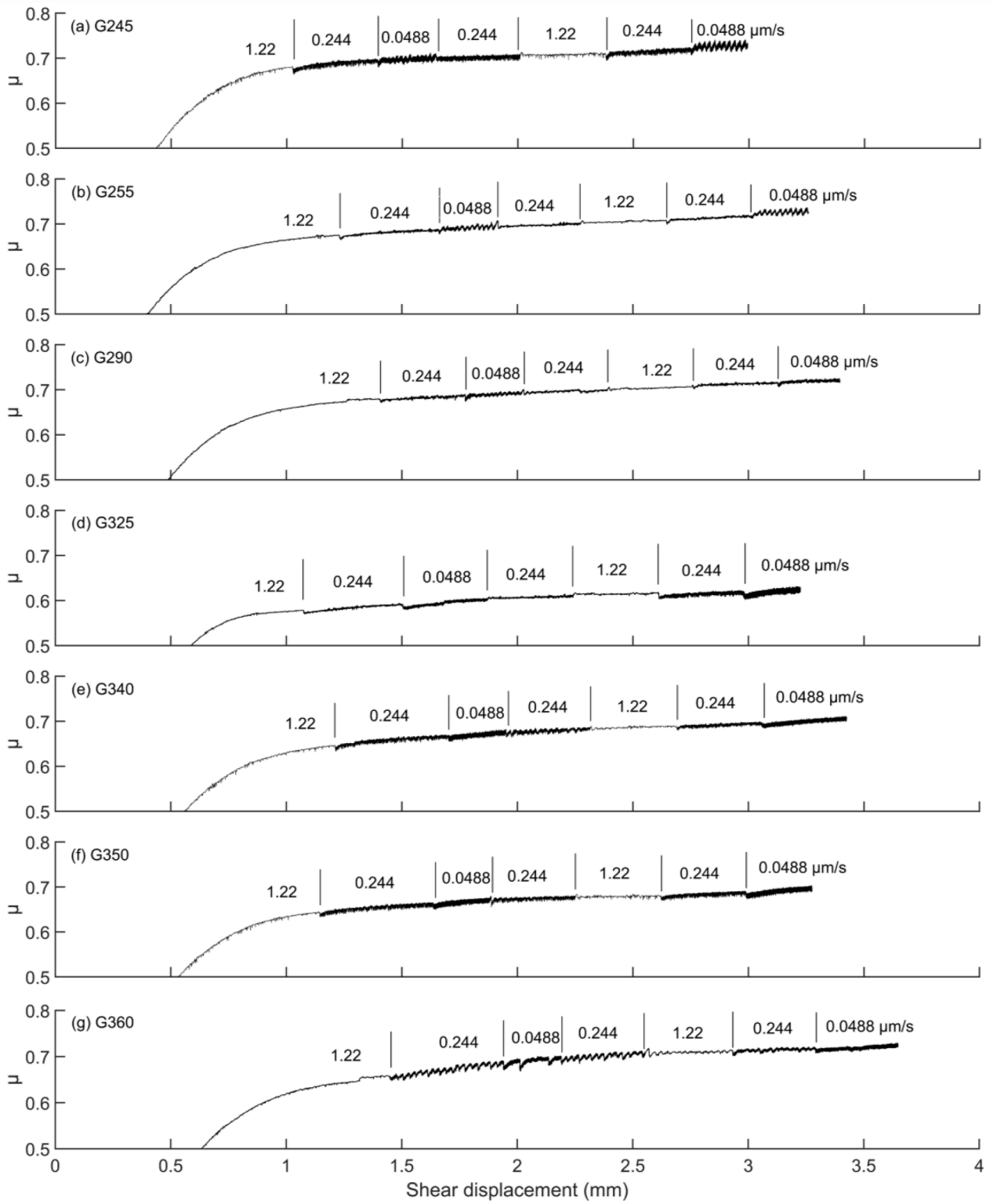

Fig. 4. Coefficient of friction versus the shear displacement for tests: (a) G245, (b) G255, (c) G290, (d) G325, (e) G340, (f) G350 and (g) G360. The shear velocities are marked above the curves.

behaviors. Our results are in accordance with the frictional stability reported for granite gouges at similar temperatures (An et al., 2021).

3.2. Temperature dependence of granite gouge

To examine the temperature dependence of the granite gouge, we conducted two more experiments at elevated temperatures (Testing ID: G245t and G340t) on gouges 245# and 340# with the results shown in Figs. 6-7. For gouge 245#, the temperature was elevated from 150 to 185℃. This temperature variation exerts nearly no influence on the frictional strength and stability–only a small increase in the values of (*a-b*) at lower shear velocities (Fig. 6). Similar results can be observed for gouge 340# when the temperature was increased from 215 to 250℃ (Fig. 7). These results indicate that the granite gouges could maintain

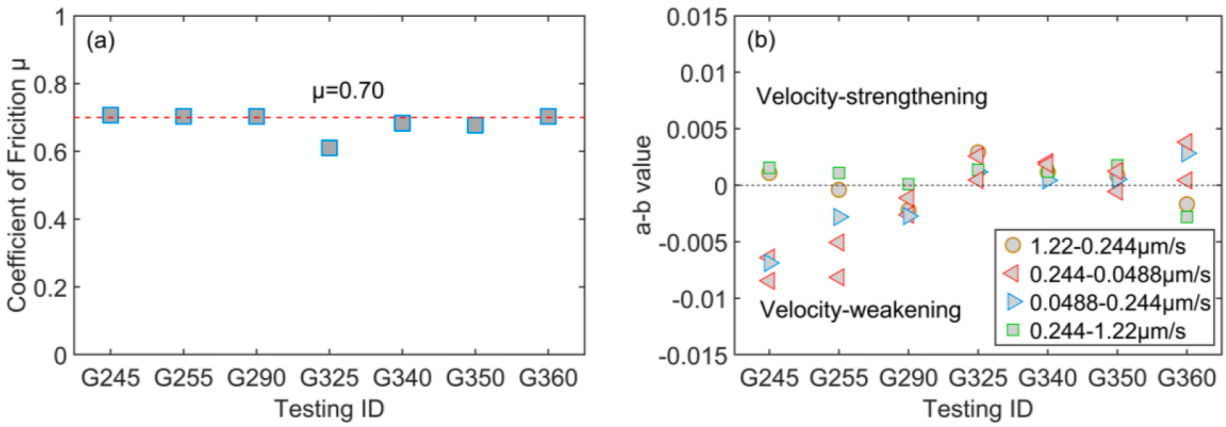

Fig. 5. (a) Coefficient of friction (μ) and (b) frictional stability (a - b) of the seven granite gouges. The coefficient of friction in each test was evaluated at the second shear velocity of 1.22 μm/s. The legend in (b) indicates the shear velocities.

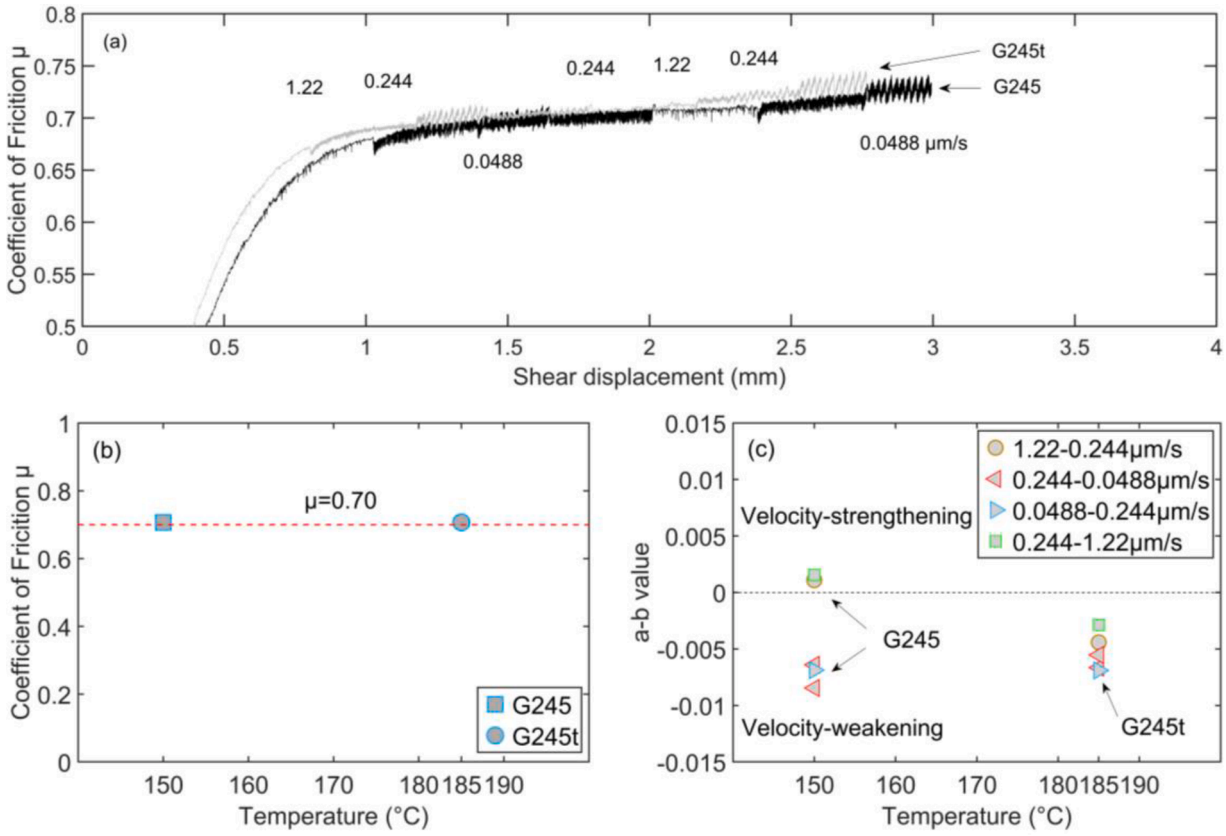

Fig. 6. Comparison of results for experiments G245 and G245t: (a) friction-displacement curves, (b) coefficient of friction (μ) and (c) frictional stability (a - b).

their frictional properties within a window of elevated temperature of <35℃ within the *in-situ* temperature range.

Our results coincide with the typical temperature dependence of wet granite gouges (Blanpied et al., 1991; Kolawle et al., 2019; An et al., 2022) (Fig. 8), i.e., hydrothermal granite gouges exhibit velocity-weakening behaviors at ~150℃ then the values of (a-b) increase with elevated temperature, and finally a transition to velocity-strengthening above 250℃ (Blanpied et al., 1991, 1995). The temperature of the Gonghe geothermal reservoir covered from 2550 m to ~3700 m in depth is included in the weakening temperature range of granite faults.

The velocity-weakening behaviors at high temperatures (<250℃) within granite gouges can be interpreted properly by a widely accepted theory based on a microphysical model advanced in Niemeijer & Spiers (2007), den Hartog et al. (2012), and den Hartog & Spiers (2013): High temperature contributes to promoting gouge compaction and porosity decrease by accelerating the rate of pressure solution. Under this condition, increasing shear velocity can facilitate shear dilation, resulting in a higher porosity and lower frictional strength. Reduced strength reflects a velocity-weakening behavior which corresponds to unstable slip and potential seismicity.

3.3. *Implication for geothermal exploitation*

Our results are significant in understanding the clusters of injection-induced earthquakes in the Gonghe Basin. Our results confirm that

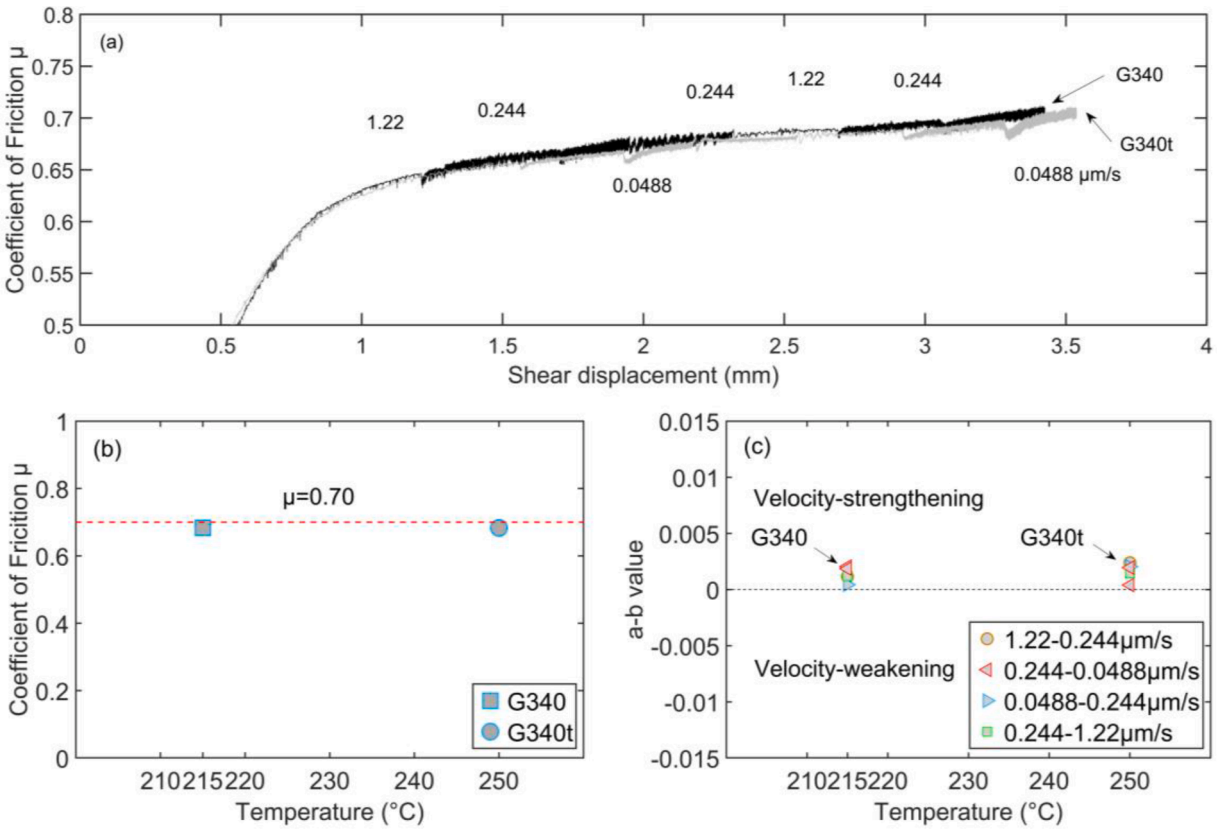

Fig. 7. Comparison of results for experiments G340 and G340t: (a) friction-displacement curves, (b) coefficient of friction (μ) and (c) frictional stability (a - b).

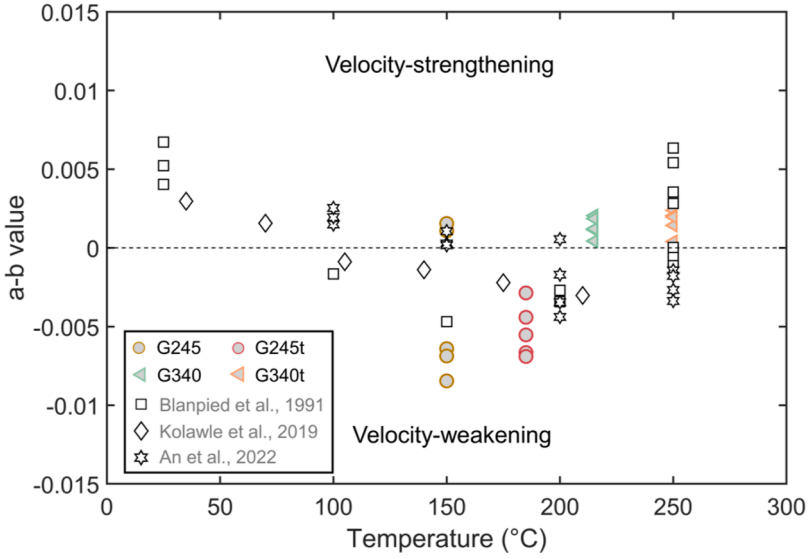

Fig. 8. Frictional stability (a - b) for granite gouges (Test IDs: G245, G245t, G340 and G340t), and other reported gouges at different temperatures. Colored dots and triangles mark the results in our study. The hollow squares, diamonds and hexagrams represent the results of Westerly granite gouges (Blanpied et al., 1991), Troy granite gouges (Kolawle et al., 2019) and Pohang granodiorite gouges (An et al., 2022) at hydrothermal conditions, respectively.

gouge-filled pre-existing faults in granite are potentially unstable at *in-situ* temperature and pressure conditions and indicate that the all-depth reservoir can be a seismogenic zone with potential seismic hazards. Under this condition, there are potentially two separate and additive destabilizing environmental factors during fluid injection (i.e., pore fluid pressure and temperature variations) that may further weaken the proven weakened granite faults at *in-situ* conditions. Firstly, increasing pore fluid pressure caused by large injection fluid volume can reactivate pre-existing faults by reducing effective normal stress (Guglielmi et al., 2015), even a minor change in pore fluid pressure reaches the critical stress state and promotes unstable slip (Scuderi et al., 2017). Pore fluid pressure heterogeneity (e.g., local fluid volume accumulation (Rutter and Hackston, 2017; Ji and Wu et al., 2020) and high injection rate (Passelègue et al., 2018; Ji et al., 2022)) is also a vital promoter for fracture instability, and fracture rupture could extend to the unpressurized area (Jia et al., 2020) and continue to after injection period

(Passelègue et al., 2018). Secondly, the injection of cold fluid into hot dry rocks could result in contractile thermoelastic strains and may also induce seismicity (Rawal and Ghassemi, 2014; Yu et al., 2018; Im et al., 2021; Gan and Elsworth., 2014a & 2014b). On the contrary, Jeanne et al. (2017) found that the cooling stress could prevent shear reactivation of the pre-existing fractures on some particular configurations. Ji et al. (2022) also suggested that a high temperature could facilitate unstable fault slip by accelerating hydrothermal reactions and enhancing fault healing, and the seismic magnitude is positively correlated with reservoir temperature. Thirdly, de Simone et al. (2017) highlighted the coupled effects of both pore fluid pressure transfer and thermo-poroelastic on inducing seismicity during injection. Pore pressure increase and thermal unclamping could also promote aseismic creep, indicating a larger seismogenic zone (Im and Avouac, 2021). Pore fluid pressure can also be elevated by the high temperature at a deeper reservoir zone, resulting in thermal pressurization and more serious seismic hazards (Ji et al., 2022).

During the stimulation of well GR1 by high pressure fluid injection for hydraulic fracturing, nearly 1300 seismic events with magnitudes in the range 0–2.0 (M_L) were detected (Chen et al., 2021) - the earthquake locations and their distribution are shown in Fig. 9. The maximum event magnitude (M_L) is nearly 2.0 although most seismic events have magnitudes below 0. The microearthquakes are mainly distributed within the depth range 3400–4000 m, and approximately within a circle of 400 m radius from well GR1 horizontally. This markable distribution of microseismic events highlights the significant weakening effect of the injection. However, districts without detected seismic events cannot be considered as aseismic. The injection can be defined as a ``blasting fuse'' to reactivate pre-existing fractures/faults already with velocity-weakening behaviors and an unstable slip trend, resulting in induced seismic events in neighboring regions.

Granite faults exhibiting velocity-weakening behaviors in the Gonghe geothermal reservoir provide necessary but insufficient conditions for instability and the triggering of seismicity. The earthquake distribution around well GR1 after injection confirms that effects such as effective stress decreasing and thermal destressing caused by injection are sufficient in this regard, and are an essential factor for the triggering of induced earthquakes during hydraulic fracturing. Thus, monitoring and exploring the stress and temperature conditions of a geothermal reservoir and the stability of pre-existing faults are of great significance before exploitation to reduce seismic hazards.

4. Conclusions

We report the results of shear experiments on powered granite gouges recovered from the Gonghe geothermal reservoir to understand mechanisms of fault remobilization and the potential for seismicity. Drilling cores recovered from well GR1, piercing the reservoir, are dominated by quartz and feldspar with a high relative content of chlorite. Experiments were conducted under *in-situ* hydrothermal conditions

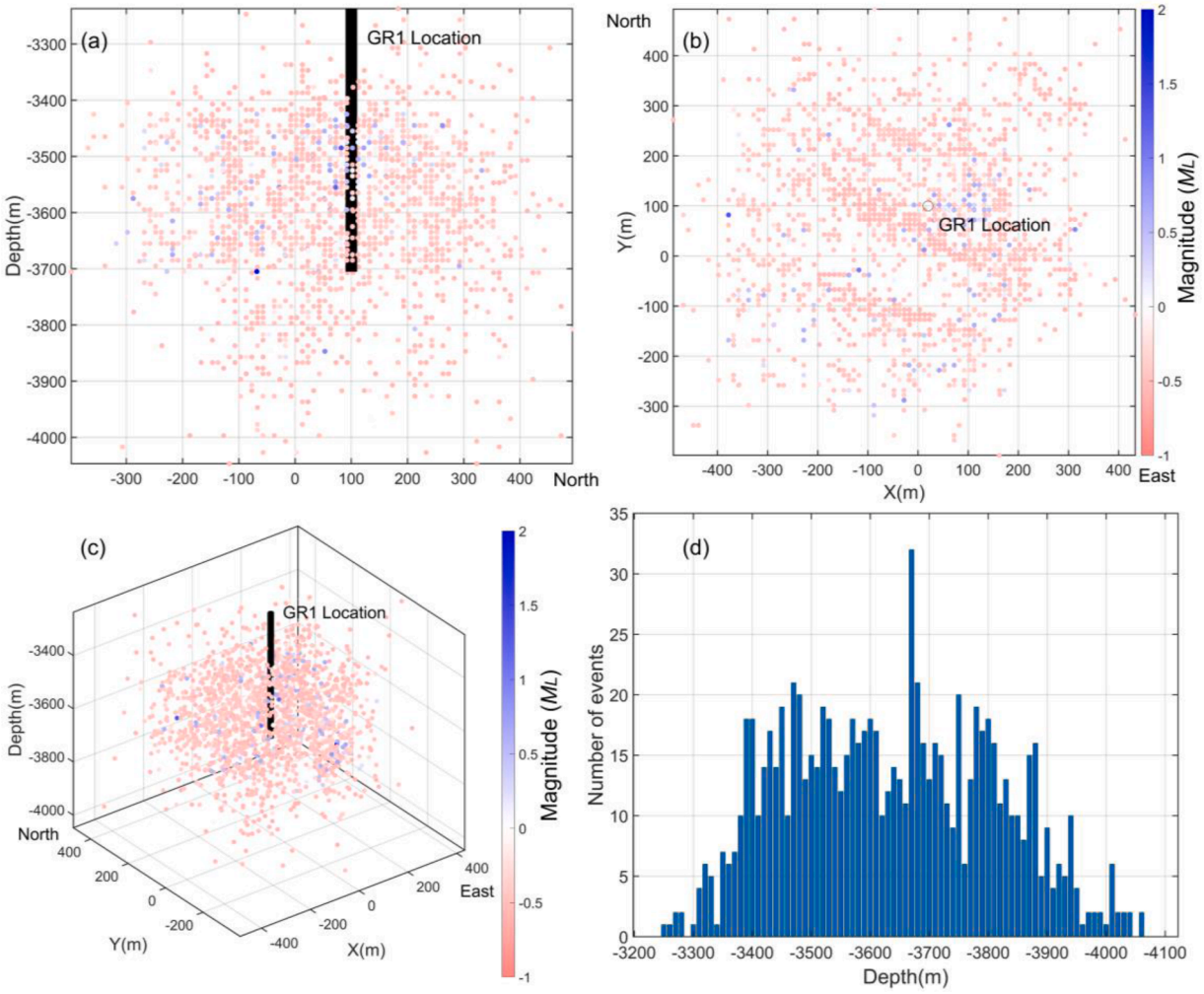

Fig. 9. Distribution of earthquakes during the hydraulic fracturing of well GR1: (a) horizontal view looking E-W, (b) plan view, (c) perspective view, and (d) distribution of the earthquake number with depth.

and the first- and second-order frictional parameters evaluated consistent with rate- and state-friction. The granite gouges all return high frictional strengths (~0.70) and velocity-neutral to slightly velocity-weakening behavior at hydrothermal conditions, indicating the potential for unstable fault slip. These observations of potential instability are congruent with observations of low-levels of seismicity during hydraulic fracturing stimulation of the site. Small temperature variations (<35℃), relative to measured at in-situ conditions, are shown to exert a negligible control on either fault frictional strength or stability.

CRediT authorship contribution statement

Fengshou Zhang: Methodology, Supervision, Validation, Writing – review & editing. **Shutian Cao:** Conceptualization, Investigation, Methodology, Writing – original draft. **Mengke An:** Data curation, Validation, Writing – review & editing. **Chongyuan Zhang:** Resources. **Derek Elsworth:** Supervision, Writing – review & editing.

Declaration of Competing Interest

The authors declare that they have no known competing financial interests or personal relationships that could have appeared to influence the work reported in this paper.

Data availability

Data will be made available on request.

Acknowledgments

This research is funded by the National Natural Science Foundation of China (42077247, 42107163), the China Postdoctoral Science Foundation (2021M692448, 2022T150483), and the Fundamental Research Funds for the Central Universities. DE acknowledges support from the G. Albert Shoemaker endowment. We appreciate the assistance of Changrong He and Wenming Yao in lab.

References

An, M., Zhang, F., Min, K.B., Elsworth, D., He, C., Zhao, L., 2022. Frictional stability of metamorphic epidote in granitoid faults under hydrothermal conditions and implications for injection-induced seismicity. J. Geophys. Res. Solid Earth 127 (3), 1–18. https://doi.org/10.1029/2021JB023136.

An, M., Zhang, F., Min, K.B., Elsworth, D., Marone, C., He, C., 2021. The potential for low-grade metamorphism to facilitate fault instability in a geothermal reservoir. Geophys. Res. Lett. 48 (11) https://doi.org/10.1029/2021GL093552.

Beeler, N.M., Rubin, A., Bhattacharya, P., Kilgore, B., Tullis, T., 2022. Apparent age dependence of the fault weakening distance in rock friction. J. Geophys. Res. Solid Earth 127 (1), 1–32. https://doi.org/10.1029/2021JB022772.

Bird, D.K., Spieler, A.R., 2004. Epidote in geothermal systems. Rev. Mineral. Geochem. 56, 235–300. https://doi.org/10.2138/gsrmg.56.1.235.

Blanpied, M.L., Lockner, D.A., Byerlee, J.D., 1991. Fault stability inferred from granite sliding experiments at hydrothermal conditions. Geophys. Res. Lett. 18 (4), 609–612. https://doi.org/10.1029/91GL00469.

Blanpied, M.L., Lockner, D.A., Byerlee, J.D., 1995. Frictional slip of granite at hydrothermal conditions. J. Geophys. Res. Solid Earth 100 (B7), 13045–13064. https://doi.org/10.1029/95JB00862.

Brace, W.F., Byerlee, J.D., 1966. Stick-slip as a mechanism for earthquakes. Science 153 (3739), 990–992. https://doi.org/10.1126/science.153.3739.990.

Breede, K., Dzebisashvili, K., Liu, X., Falcone, G., 2013. A systematic review of enhanced (or engineered) geothermal systems: past, present and future. Geothermal Energy 1 (1). https://doi.org/10.1186/2195-9706-1-4.

Buijze, L., Guo, Y., Niemeijer, A.R., Ma, S., Spiers, C.J., 2020. Nucleation of stick-slip instability within a large-scale experimental fault: effects of stress heterogeneities due to loading and gouge layer compaction. J. Geophys. Res. Solid Earth 125 (8). https://doi.org/10.1029/2019JB018429.

Carpenter, B.M., Ikari, M.J., Marone, C., 2016. Laboratory observations of time-dependent frictional strengthening and stress relaxation in natural and synthetic fault gouges. J. Geophys. Res. Solid Earth 121 (2), 1183–1201. https://doi.org/10.1002/2015JB012136.

Chen, Z., Zhao, F., Sun, F., Lv, H., Wang, C., Wu, H., et al., 2021. Hydraulic fracturing-induced seismicity at the hot dry rock site of the Gonghe Basin in China. Acta Geologica Sinica-English Edition 95 (6), 1835–1843. https://doi.org/10.1111/1755-6724.14883.

den Hartog, S.A.M., Niemeijer, A.R., Spiers, C.J., 2012. New constraints on megathrust slip stability under subduction zone P-T conditions. Earth Planet. Sci. Lett. 353–354, 240–252. https://doi.org/10.1016/j.epsl.2012.08.022.

den Hartog, S.A.M., Spiers, C.J., 2013. Influence of subduction zone conditions and gouge composition on frictional slip stability of megathrust faults. Tectonophysics 600, 75–90. https://doi.org/10.1016/j.tecto.2012.11.006.

de Simone, S., Carrera, J., Vilarrasa, V., 2017. Superposition approach to understand triggering mechanisms of post-injection induced seismicity. Geothermics 70, 85–97. https://doi.org/10.1016/j.geothermics.2017.05.011.

Dieterich, J.H., 1979. Modeling of rock friction: 1. Experimental results and constitutive equations. J. Geophys. Res. 84 (B5), 2161–2168. https://doi.org/10.1029/JB084iB05p02161.

Gan, Q., Elsworth, D., 2014a. Thermal drawdown and late-stage seismic-slip fault reactivation in enhanced geothermal reservoirs. J. Geophys. Res. Solid Earth 119 (12), 8936–8949. https://doi.org/10.1002/2014JB011323.

Gan, Q., Elsworth, D., 2014b. Analysis of fluid injection-induced fault reactivation and seismic slip in geothermal reservoirs. J. Geophys. Res. Solid Earth 119 (4), 3340–3353. https://doi.org/10.1002/2013JB010679.

Giacomel, P., Ruggieri, R., Scuderi, M.M., Spagnuolo, E., Di Toro, G., Collettini, C., 2021. Frictional properties of basalt experimental faults and implications for volcano-tectonic settings and geo-energy sites. Tectonophysics 811 (B3). https://doi.org/10.1016/j.tecto.2021.228883.

Grigoli, F., Cesca, S., Rinaldi, A.P., Manconi, A., López-Comino, J.A., Clinton, J.F., et al., 2018. The November 2017 Mw 5.5 Pohang earthquake: a possible case of induced seismicity in South Korea. Science 360 (6392), 1003–1006. https://doi.org/10.1126/science.aat2010.

Guglielmi, Y., Cappa, F., Avouac, J.P., Henry, P., Elsworth, D., 2015. Seismicity triggered by fluid injection-induced aseismic slip. Science 348 (6240), 1224–1226. https://doi.org/10.1126/science.aab0476.

He, C., Yao, W., Wang, Z., Zhou, Y., 2006. Strength and stability of frictional sliding of gabbro gouge at elevated temperatures. Tectonophysics 427 (1–4), 217–229. https://doi.org/10.1016/j.tecto.2006.05.023.

Ikari, M.J., Saffer, D.M., Marone, C., 2009. Frictional and hydrologic properties of clay-rich fault gouge. J. Geophys. Res. (B5), 114. https://doi.org/10.1029/2008JB006089.

Im, K., Avouac, J.P., 2021. On the role of thermal stress and fluid pressure in triggering seismic and aseismic faulting at the Brawley Geothermal Field, California. Geothermics 97. https://doi.org/10.1016/j.geothermics.2021.102238.

Im, K., Avouac, J.P., Heimisson, E.R., Elsworth, D., 2021. Ridgecrest aftershocks at Coso sippressed by thermal destressing. Nature 595 (7865), 70–74. https://doi.org/10.1038/s41586-021-03601-4.

Jeanne, P., Rutqvist, J., Dobson, P.F., 2017. Influence of injection-induced cooling on deviatoric stress and shear reactivation of preexisting fractures in Enhanced Geothermal Systems. Geothermics 70, 367–375. https://doi.org/10.1016/j.geothermics.2017.08.003.

Ji, Y., Hofmann, H., Rutter, E.H., Zang, A., 2022. Transition from slow to fast injection-induced slip of an experimental fault in granite promoted by elevated temperature. Geophys. Res. Lett. (23), 49. https://doi.org/10.1029/2022GL101212.

Ji, Y., Wang, L., Hofmann, H., Kwiatek, G., Dresen, G., 2022. High-rate fluid injection reduces the nucleation length of laboratory earthquakes on critically stressed faults in granite. Geophys. Res. Lett. 49 (23), 1–13. https://doi.org/10.1029/2022GL100418.

Ji, Y., Wu, W., 2020. Injection-driven fracture instability in granite: mechanism and implications. Tectonophysics 791. https://doi.org/10.1016/j.tecto.2020.228572.

Jia, Y., Wu, W., Kong, X.Z., 2020. Injection-induced slip heterogeneity on faults in shale reservoirs. Int. J. Rock Mech. Min. Sci. 131 https://doi.org/10.1016/j.ijrmms.2020.104363.

Jiang, Y., Li, B., Wang, C., Song, Z., Yan, B., 2022. Advances in development of shear-flow testing apparatuses and methods for rock fractures: a review. Rock Mech. Bull. 1 (1), 100005 https://doi.org/10.1016/j.rockmb.2022.100005.

Johnson, T., Wu, F.T., Scholz, C.H., 1973. Source parameters for stick-slip and for earthquakes. Science 179 (4070), 278–279. https://doi.org/10.1126/science.179.4070.278.

Kang, F., Li, Y., Tang, C., 2021. Grain size heterogeneity controls strengthening to weakening of granite over high-temperature treatment. Int. J. Rock Mech. Min. Sci. 145 https://doi.org/10.1016/j.ijrmms.2021.104848.

Kim, K.H., Ree, J.H., Kim, Y.H., Kim, S., Kang, S.Y., Seo, W., 2018. Assessing whether the 2017 Mw 5.4 Pohang earthquake in South Korea was an induced event. Science 360 (6392), 1007–1009. https://doi.org/10.1126/science.aat6081.

Kolawole, F., Johnston, C.S., Morgan, C.B., Chang, J.C., Marfurt, K.J., Lockner, D.A., et al., 2019. The susceptibility of Oklahoma's basement to seismic reactivation. Nat. Geosci. 12 (10), 839–844. https://doi.org/10.1038/s41561-019-0440-5.

Kovac, K.M., Moore, J.N., Lutz, S.J., 2005. Geologic framework of the East Flank, Coso geothermal field: implications for EGS development. In: Proceedings 30th Workshop on Geothermal Engineering. Stanford University, p. 486, 492.

Kwon, S., Xie, L., Park, S., Kim, K.I., Min, K.B., Kim, K.Y., et al., 2019. Characterization of 4.2-km-deep fractured granodiorite cores from Pohang geothermal reservoir, Korea. Rock Mech. Rock Eng. 52 (3), 771–782. https://doi.org/10.1007/s00603-018-1639-2.

Ladner, F., Häring, M.O., 2009. Hydraulic characteristics of the Basel 1 enhanced geothermal system. GRC Trans. 33, 199–203.

Liu, B., Zhao, H., Jin, H., Chen, F., 2020. Holocene moisture variation recorded by aeolian sand-palaeosol sequences of the Gonghe Basin, northeastern Qinghai-Tibetan

Plateau, China. Acta Geologica Sinica-English Edition 94 (3), 668–681. https://doi.org/10.1111/1755-6724.14541.
Lockner, D.A., Summers, R., Byerlee, J.D., 1986. Effects of temperature and sliding rate on frictional strength of granite. Pure Appl. Geophys. 124 (3), 445–469. https://doi.org/10.1007/BF00877211.
Majer, E.L., Baria, R., Stark, M., Oates, S., Bommer, J., Smith, B., et al., 2007. Induced seismicity associated with enhanced geothermal systems. Geothermics 36 (3), 185–222. https://doi.org/10.1016/j.geothermics.2007.03.003.
Marone, C., Kilgore, B., 1993. Scaling of the critical slip distance for seismic faulting with shear strain in fault zones. Nature 362 (6421), 618–621. https://doi.org/10.1038/362618a0.
Marone, C., Raleigh, C.B., Scholz, C.H., 1990. Frictional behavior and constitutive modeling of simulated fault gouge. J. Geophys. Res. 95 (B5), 7007–7025. https://doi.org/10.1029/JB095iB05p07007.
Marone, C., Scholz, C.H., 1989. Particle-size distribution and microstructures within simulated fault gouge. J. Struct. Geol. 11 (7), 799–814. https://doi.org/10.1016/0191-8141(89)90099-0.
Mitchell, E.K., Fialko, Y., Brown, K.M., 2016. Velocity-weakening behavior of Westerly granite at temperature up to 600 °C. J. Geophys. Res. Solid Earth 121 (9), 6932–6946. https://doi.org/10.1002/2016JB013081.
Moore, D.E., Lockner, D.A., Byerlee, J.D., 1994. Reduction of permeability in granite at elevated temperatures. Science 265 (5178), 1558–1561. https://doi.org/10.1126/science.265.5178.1558.
Morrow, C.A., Moore, D.E., Lockner, D.A., 2001. Permeability reduction in granite under hydrothermal conditions. J. Geophys. Res. Atmos. 106 (B12), 30551–30560.
Niemeijer, A.R., Spiers, C.J., 2007. A microphysical model for strong velocity weakening in phyllosilicate-bearing fault gouges. J. Geophys. Res. Solid Earth 112 (10), 1–12. https://doi.org/10.1029/2007JB005008.
Passelègue, F.X., Brantut, N., Mitchell, T.M., 2018. Fault reactivation by fluid injection: controls from stress state and injection rate. Geophys. Res. Lett. 45 (23), 12837–12846. https://doi.org/10.1029/2018GL080470.
Pearson, C., 1981. The relationship between microseismicity and high pore pressures during hydraulic stimulation experiments in low permeability granitic rocks. J. Geophys. Res. 86 (NB9), 7855–7864. https://doi.org/10.1029/JB086iB09p07855.
Rawal, C., Ghassemi, A., 2014. A reactive thermo-poroelastic analysis of water injection into an enhanced geothermal reservoir. Geothermics 50, 10–23. https://doi.org/10.1016/j.geothermics.2013.05.007.
Rice, J.R., 1983. Constitutive relations for fault slip and earthquake instabilities. Pure Appl. Geophys. 121 (3), 443–475. https://doi.org/10.1007/BF02590151.
Roux, S., Hansen, A., Herrmann, H.J., Vilotte, J.P., 1993. A model for gouge deformation - implications for remanent magnetization. Geophys. Res. Lett. 20 (14), 1499–1502. https://doi.org/10.1029/93GL00680.
Ruina, A., 1983. Slip instability and state variable friction laws. J. Geophys. Res. 88 (B12), 10359–10370. https://doi.org/10.1029/JB088iB12p10359.
Rutter, E., Hackston, A., 2017. On the effective stress law for rock-on-rock frictional sliding, and fault slip triggered by means of fluid injection. Philos. Trans. R. Soc. A Math. Phys. Eng. Sci. 375 (2103) https://doi.org/10.1098/rsta.2016.0001.
Scholz, C.H., 1990. The Mechanics of Earthquakes and Faulting. Cambridge University Press. https://doi.org/10.1017/9781316681473.
Scuderi, M.M., Collettini, C., Marone, C., 2017. Frictional stability and earthquake triggering during fluid pressure stimulation of an experimental fault. Earth Planet. Sci. Lett. 477, 84–96. https://doi.org/10.1016/j.epsl.2017.08.009.
Stesky, R.M., 1978. Mechanisms of high temperature frictional sliding in Westerly granite. Can. J. Earth Sci. 15 (3), 361–375. https://doi.org/10.1139/e78-042.
Sun, Q., Colin, C., 2014. Paleoclimate and paleoenvironment of Gonghe Basin, Qinghai-Tibet Plateau, during the Lastdeglacial: weathering, erosion and vegetation cover affect clay mineral formation. ACTA Geologica Sinica-English Edition 88 (2), 647–660. https://doi.org/10.1111/1755-6724.12220.
Talarico, F., Kleinschmidt, G., 2003. The mertz shear zone (George v land): implications for australia/antarctica correlations and east antarctic craton/ross orogen relationships. Netherlands J. Geosci. 91 (4), 1–3. https://doi.org/10.1007/BF00435158.
Tembe, S., Lockner, D.A., Wong, T.F., 2010. Effect of clay content and mineralogy on frictional sliding behavior of simulated gouges: binary and ternary mixtures of quartz, illite, and montmorillonite. J. Geophys. Res. Solid Earth 115 (3), 1–22. https://doi.org/10.1029/2009JB006383.
Vidal, J., Genter, A., 2018. Overview of naturally permeable fractured reservoirs in the central and southern Upper Rhine Graben: insights from geothermal wells. Geothermics 74, 57–73. https://doi.org/10.1016/j.geothermics.2018.02.003.
Vrolijk, P., Van Der Pluijm, B.A, 1999. Clay gouge. J. Struct. Geol. 21 (8–9), 1039–1048. https://doi.org/10.1016/S0191-8141(99)00103-0.
Wehrens, P., Berger, A., Peters, M., Spillmann, T., Herwegh, M., 2016. Deformation at the frictional-viscous transition: evidence for cycles of fluid-assisted embrittlement and ductile deformation in the granitoid crust. Tectonophysics 693, 66–84. https://doi.org/10.1016/j.tecto.2016.10.022.
Ye, Z., Ghassemi, A., 2018. Injection-induced shear slip and permeability enhancement in granite fractures. J. Geophys. Res. Solid Earth 123 (10), 9009–9032. https://doi.org/10.1029/2018JB016045.
Yu, C., Vaclav, V., Petra, A., Marco, B., 2018. Moment tensors of induced microearthquakes in the Geysers geothermal reservoir from broadband seismic recordings: implications for faulting regime, stress tensor, and fluid pressure. J. Geophys. Res. Solid Earth 123 (10), 8748–8766. https://doi.org/10.1029/2018JB016251.
Zhang, F., Huang, R., An, M., Min, K.B., Elsworth, D., Hofmann, H., Wang, X., 2022. Competing controls of effective stress variation and chloritization on friction and stability of faults in granite: implications for seismicity triggered by fluid injection. J. Geophys. Res. Solid Earth 127 (8). https://doi.org/10.1029/2022JB024310.
Zhang, S., Yan, W., Li, D., Jia, X., Zhang, S., Li, S., et al., 2018. Characteristics of geothermal geology of the Qiabuqia HDR in Gonghe Basin, Qinghai Province. Geol. China 45 (6), 1087–1102. https://doi.org/10.12029/gc20180601 in Chinese with English abstract.
Zhu, J., Hu, K., Lu, X., Huang, X., Liu, K., Wu, X., 2015. A review of geothermal energy resources, development, and applications in China: current status and prospects. Energy 93, 466–483. https://doi.org/10.1016/j.energy.2015.08.098.
Zoback, M.D., Harjes, H.P., 1997. Injection-induced earthquakes and crustal stress at 9 km depth at the KTB deep drilling site, Germany. J. Geophys. Res. Solid Earth 102 (B8), 18477–18491. http://doi.org/10.1029/96JB02814.